

**Quantum state engineering of spin-orbit-coupled ultracold atoms in a Morse potential**Yue Ban,<sup>1</sup> Xi Chen,<sup>2</sup> J. G. Muga,<sup>2,3</sup> and E. Ya Sherman<sup>3,4</sup><sup>1</sup>*Department of Electronic Information Materials, Shanghai University, 200444 Shanghai, People's Republic of China*<sup>2</sup>*Department of Physics, Shanghai University, 200444 Shanghai, People's Republic of China*<sup>3</sup>*Departamento de Química-Física, UPV/EHU, Apartado 644, 48080 Bilbao, Spain*<sup>4</sup>*IKERBASQUE, Basque Foundation for Science, 48011 Bilbao, Spain*

(Received 13 September 2014; published 5 February 2015)

Achieving full control of a Bose-Einstein condensate can have valuable applications in metrology, quantum information processing, and quantum condensed matter physics. We propose protocols to simultaneously control the internal (related to its pseudospin-1/2) and motional (position-related) states of a spin-orbit-coupled Bose-Einstein condensate confined in a Morse potential. In the presence of synthetic spin-orbit coupling, the state transition of a noninteracting condensate can be implemented by Raman coupling and detuning terms designed by invariant-based inverse engineering. The state transfer may also be driven by tuning the direction of the spin-orbit-coupling field and modulating the magnitude of the effective synthetic magnetic field. The results can be generalized for interacting condensates by changing the time-dependent detuning to compensate for the interaction. We find that a two-level algorithm for the inverse engineering remains numerically accurate even if the entire set of possible states is considered. The proposed approach is robust against the laser-field noise and systematic device-dependent errors.

DOI: [10.1103/PhysRevA.91.023604](https://doi.org/10.1103/PhysRevA.91.023604)

PACS number(s): 03.75.Kk, 37.10.Gh, 32.80.Qk, 05.30.Jp

**I. INTRODUCTION**

Coherent high-fidelity control of quantum systems is a fundamental task in many areas of atomic, molecular, optical, and condensed matter physics. Algorithms of such a control can be applied in metrology, interferometry, and quantum information processing. Specifically, achieving fast and stable manipulation of ultracold ensembles of bosonic and fermionic atoms by driving the system from an initial to a target state with high fidelity has been a major research goal during the past two decades.

Motional state control of localized atoms, in particular, can be achieved by techniques similar to those applied for trapped ions or via trap deformations [1,2]. A synthetic spin-orbit (SO) coupling has also been proposed to control the orbital motion of atoms [3,4].

In recent years, laser control techniques have successfully produced synthetic SO coupling in ultracold ensembles of neutral atoms such as Bose-Einstein condensates (BECs) [5,6] and Fermi gases [7–9]. SO-coupled BECs (see recent reviews [10–12]) allow for control of several tunable parameters. The combination of tunable SO coupling with interatomic interactions leads to novel phenomena unprecedented in conventional condensed matter physics. SO-coupled condensates have been used, for example, to study and control spin dynamics in processes such as spin relaxation [13], *Zitterbewegung* [14,15], spin resonance, and the spin-Hall effect. Tunable Landau-Zener transitions in an SO-coupled BEC were experimentally studied [16].

In this paper, we study the control of the dynamics of an SO-coupled BEC confined in a Morse potential by inverse engineering [17,18] the control parameters. In this analytically solvable potential, the level spacing decreases as the energy approaches the continuous spectrum and its spatial asymmetry implies a displacement of the center of mass for transitions between vibrational states. In the configurations producing experimentally synthetic SO coupling [6], the control of the

internal states can be implemented by tuning the coupling of the atomic pseudospin to the laser field, similarly to the invariant-based inverse engineering for spin control in quantum dots [19]. For example, the amplitude of the external synthetic magnetic field and the direction of the SO-coupling field can be chosen as the tunable parameters to control simultaneously the internal state and the position transfer, resulting from the effect of the synthetic SO coupling on the orbital motion.

The paper is organized as follows: In Sec. II, we introduce the model, reduce it to the effective two-level system, and formulate the initial and the target states of the transfer. In Sec. III, time-dependent Raman coupling and Raman detuning are designed to control internal and motional states by invariant-based inverse engineering for a noninteracting condensate. Here we demonstrate that the designed two-level algorithm is applicable and gives a high fidelity for a more complicated multilevel system as well. In Sec. IV, the direction of the SO-coupling field and the level detuning are designed to achieve the state transfer. The inverse engineering method is generalized here for an interacting BEC by using a simple ansatz of the state evolution on the Bloch sphere. The robustness of this protocol with respect to noise and systematic errors is discussed in Sec. V, and a short summary is provided in Sec. VI.

**II. MODEL AND HAMILTONIAN**

We consider ultracold bosonic atoms trapped in a one-dimensional (1D) Morse potential [20] of the form

$$U(x) = A(e^{-2ax} - 2e^{-ax}), \quad (1)$$

as shown in Fig. 1, where the characteristic parameters  $A$  and  $a$  have units of energy and inverse length, respectively. For small values of  $a$ , this potential can host many bound states, while it becomes shallow and contains only a continuous spectrum at large  $a$ . In the deep potential, low-energy states

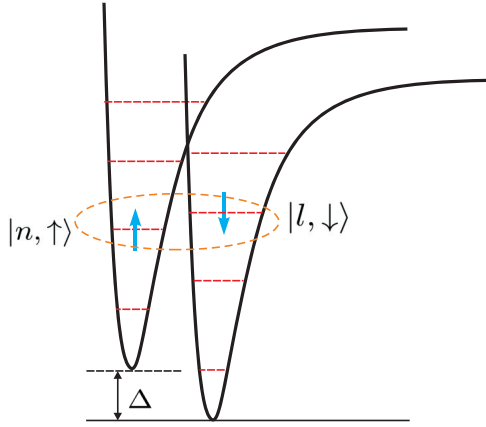


FIG. 1. (Color online) Schematic of bosonic atoms trapped in a Morse potential in an external effective magnetic field. The Kramers degeneracy here was eliminated and the energy gap between  $|n, \uparrow\rangle$  and  $|l, \downarrow\rangle$  is much less than the distance to the neighboring orbital states.

are characterized by the harmonic frequency near the trap minimum  $\omega = \sqrt{2Aa^2/M}$  (where  $M$  is the mass of an atom) with oscillator length  $l_c = \sqrt{\hbar/M\omega}$  (see Ref. [21] for realistic values of the parameters). The Morse potential has traditionally been considered a model for diatomic molecules, with coexisting unbound and bound states. In the physics of cold atoms, the Morse potential can be produced with two evanescent light waves [22]. Due to the spatial asymmetry of the potential, the state control is accompanied by atomic displacements, which can be useful for interferometric applications so that each interferometer arm is subjected to a different effect. In what follows, we put  $M \equiv \hbar \equiv 1$  and use  $a^{-1}$  and  $1/a^2$  as units for the length and time, respectively.

The normalized orbital states in  $x$ -coordinate representation have the form

$$\langle x|n\rangle = n!z^\xi \sqrt{\frac{2\xi}{\gamma(n+1)\gamma(2\eta-n)}} \exp\left(-\frac{z}{2}\right) L_n^{2\xi}(z), \quad (2)$$

with eigenvalues  $E_n = -(\eta - n - 1/2)^2/2$ , where  $\gamma(n)$  is the Euler  $\gamma$  function,  $\eta = \sqrt{2A}$ ,  $\xi = \eta - n - 1/2$ ,  $z \equiv z(x) = 2\eta \exp(-x)$ , and  $L$  is the Laguerre polynomial.

An atom moving in a 1D Morse potential (in the  $x$  direction) with a Raman laser configuration producing a pseudospin SO-coupling field pointing in the  $z$  direction is described by the Hamiltonian [6]

$$\mathcal{H}_0 = \frac{p^2}{2} + U(x) + \frac{\Omega(t)}{2}\sigma_x + \frac{\Delta(t)}{2}\sigma_z + \alpha p\sigma_z, \quad (3)$$

where  $p$  is the momentum of the atoms, the Pauli matrix vector is  $\sigma = (\sigma_x, \sigma_y, \sigma_z)$ ,  $\alpha$  is the SO-coupling strength,  $\Delta$  is the detuning from resonance (Zeeman term), and  $\Omega$  is the effective Rabi frequency of the two-level system (Raman coupling strength) [6]. For  $\Omega = 0$  the Hamiltonian  $\mathcal{H}_0$  has “spin-up” eigenstates  $|n, \uparrow\rangle = e^{-i\alpha x}|n\rangle|\uparrow\rangle$  (with eigenvalue  $E_{n,\uparrow}$ ) and “spin-down” eigenstates  $|l, \downarrow\rangle = e^{i\alpha x}|l\rangle|\downarrow\rangle$  (with eigenvalue  $E_{l,\downarrow}$ ,  $l = n + 1$ ), as shown in Fig. 1, where  $|\uparrow\rangle$  and  $|\downarrow\rangle$  are the eigenspinors of  $\sigma_z$ . In the following, different schemes of inverse engineering are proposed to transfer the

state from  $|n, \uparrow\rangle$  to  $|l, \downarrow\rangle$ . We assume that  $\Delta$  is of the order of  $|E_n - E_l|$  such that the distance  $\Delta E = |E_{n,\uparrow} - E_{l,\downarrow}|$  is much smaller than the gap between the neighboring orbital states, making the doublet of interest energetically well separated from other states. Thus, if the requested operation time  $t_f$  satisfies the condition  $t_f \gg 1/\Delta$ , one can neglect the excitation of other states, and an effective two-level system can be established to describe the state transfer in the Morse potential. In addition, later we show that algorithms developed in the two-level approximation can, with a high accuracy, be applied to multilevel systems as well.

### III. SCHEME 1: STATE TRANSITION BY TUNABLE RAMAN COUPLING AND DETUNING

To drive the state  $|n, \uparrow\rangle$ , where  $|n, \uparrow\rangle \equiv e^{-i\alpha x}|n\rangle|\uparrow\rangle$  and  $|n\rangle$  is given by Eq. (2), to  $|n + 1, \downarrow\rangle$ , the closest one in energy (see Fig. 1), we construct a  $2 \times 2$  Hamiltonian by taking the matrix elements of  $\mathcal{H}_0$  [Eq. (3)] in the basis of these two states and write it in the symmetric form

$$H_0(t) = \frac{1}{2} \begin{bmatrix} Z & X + iY \\ X - iY & -Z \end{bmatrix}, \quad (4)$$

where  $Z = E_n - E_l + \Delta(t)$  is a time-dependent “energy gap,”  $X = \Omega(t)\text{Re}[G]$ ,  $Y = \Omega(t)\text{Im}[G]$ , and  $G = \langle n|e^{2i\alpha x}|l\rangle$ . The wave function corresponding to the Hamiltonian, Eq. (4), has the form  $\psi = (\psi_1, \psi_2)^T$ , where  $\psi_1 = \langle n, \uparrow|\psi\rangle$  and  $\psi_2 = \langle l, \downarrow|\psi\rangle$ . The dynamical invariant of  $H_0$ ,

$$I(t) = \frac{\lambda_0}{2} \begin{bmatrix} \cos\theta_a & \sin\theta_a e^{i\varphi_a} \\ \sin\theta_a e^{-i\varphi_a} & -\cos\theta_a \end{bmatrix}, \quad (5)$$

where  $\lambda_0$  is a constant having the units of energy, is constructed with yet unknown orthogonal eigenstates  $|\chi_\pm(t)\rangle$ :

$$|\chi_+(t)\rangle = \begin{pmatrix} \cos\frac{\theta_a}{2} e^{i\varphi_a/2} \\ \sin\frac{\theta_a}{2} e^{-i\varphi_a/2} \end{pmatrix}, \quad (6)$$

$$|\chi_-(t)\rangle = \begin{pmatrix} \sin\frac{\theta_a}{2} e^{i\varphi_a/2} \\ -\cos\frac{\theta_a}{2} e^{-i\varphi_a/2} \end{pmatrix}. \quad (7)$$

Here  $\theta_a$  and  $\varphi_a$  are the (auxiliary) polar and the azimuthal angles for the eigenstates of the invariant. According to the Lewis-Riesenfeld theory, the solution of the Schrödinger equation,  $i\partial_t\psi = H_0(t)\psi$ , is a superposition of orthonormal “dynamical modes,”  $\psi(t) = \sum_n C_n e^{i\xi_n} |\chi_n(t)\rangle$  [23], where  $C_n$  are time-independent amplitudes and  $\xi_n$  are Lewis-Riesenfeld phases. Here, we set the trajectory of the actual state evolution along  $|\chi_+(t)\rangle$ . From the invariant condition,

$$\frac{dI(t)}{dt} \equiv i\frac{\partial I(t)}{\partial t} - [H_0(t), I(t)] = 0, \quad (8)$$

we find equations in terms of  $\theta_a$  and  $\varphi_a$ , yielding the two controllable parameters

$$\Omega(t) = -\frac{\dot{\theta}_a}{|G|\sin(\phi - \varphi_a)}, \quad (9)$$

$$\Delta(t) = E_l - E_n - \dot{\varphi}_a - \frac{\dot{\theta}_a \cos\theta_a \cos(\phi - \varphi_a)}{\sin\theta_a \sin(\phi - \varphi_a)}, \quad (10)$$

where  $\tan\phi = \text{Im}[G]/\text{Re}[G]$ .

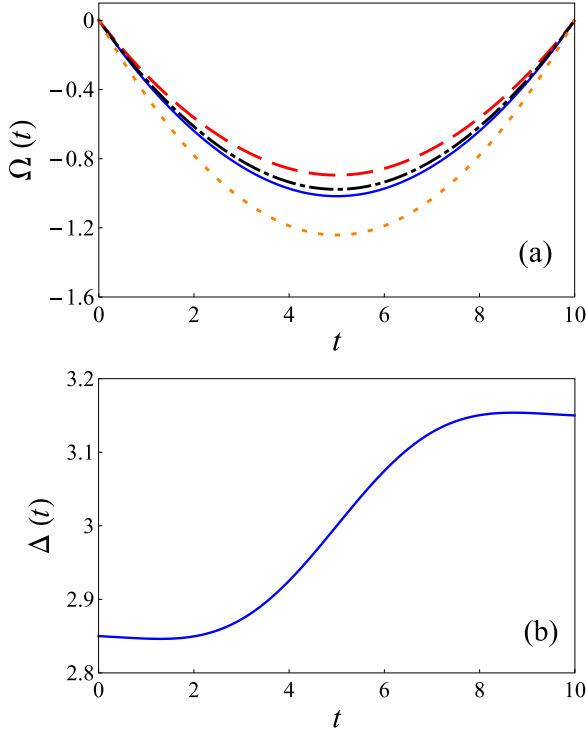


FIG. 2. (Color online) (a) Time dependence of Raman coupling strength  $\Omega$  with different SO-coupling parameters:  $\alpha = 0.8$  [solid (blue) curve],  $\alpha = 1.2$  [dashed (red) curve],  $\alpha = 1.6$  [dot-dashed (black) curve], and  $\alpha = 2$  [dotted (orange) curve]. (b) Time dependence of the level detuning  $\Delta$ . Other parameters are  $t_f = 10$  and  $c = 0.1$  in (a) and (b).

To produce the state transfer,  $\theta_a$  is set by a polynomial ansatz  $\theta_a = \sum_{n=0}^3 a_n t^n$  with boundary conditions  $\theta_a(0) = 0$ ,  $\theta_a(t_f) = \pi$ ,  $\dot{\theta}_a(0) = \dot{\theta}_a(t_f) = 0$ . These conditions imply the commutativity of the Hamiltonian and the invariant at the boundary times. Then  $\Delta(t)$  would diverge at  $t = 0$  and  $t = t_f$ . To cancel these two singularities, we impose  $\dot{\theta}_a \cot(\phi - \varphi_a) = c \sin \theta_a$ , where  $c$  is a real number. This results in  $\dot{\varphi}_a(0^+) = c$ ,  $\dot{\varphi}_a(t_f^-) = -c$  and leads to  $\Delta(0^+) = -E_n + E_l - 3c/2$  and  $\Delta(t_f^-) = -E_n + E_l + 3c/2$ .

To provide a practical example, we consider the Morse potential with  $A = 8$ . We take  $n = 0, l = 1$ , and operation time  $t_f = 10$ . The parameters  $\Omega$  and  $\Delta$  are shown in Fig. 2 for different values of  $\alpha$ . The time-dependent ‘‘energy gap’’ and detuning  $\Delta$  remain unaffected by  $\alpha$ . This is because  $\phi - \varphi_a$  and  $\dot{\varphi}_a$  depend only on  $\theta_a$ . Consequently, in transitions with the same gap at different values of  $\alpha$ , the product  $\Omega(t)G$  should remain  $\alpha$  independent. Thus, with the increase in  $\alpha$ , the absolute value  $|\Omega(t)|$  at given  $t$  first decreases and then increases, as shown in Fig. 2(a).

In the transition, the expectation value of the coordinate

$$\langle x \rangle = \langle \psi | \hat{x} | \psi \rangle \quad (11)$$

varies with time because of the asymmetry of the Morse potential (see Fig. 3).

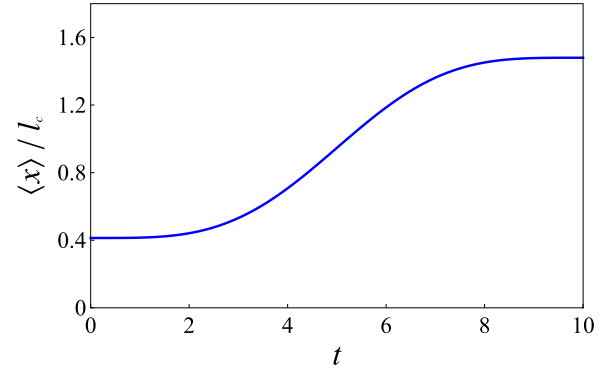


FIG. 3. (Color online) Time dependence of the expectation value of coordinate  $\langle x \rangle$  in units of  $l_c$  for noninteracting atoms, with  $t_f = 10$ ,  $\alpha = 1.6$ , and  $c = 0.1$ . The initial state is  $|0, \uparrow\rangle$  and the final one is  $|1, \downarrow\rangle$ .

The components of the resulting spin polarization,

$$P_i(t) = \langle \psi | \hat{\sigma}_i | \psi \rangle, \quad (12)$$

are given by

$$P_x = \int_{-\infty}^{+\infty} (\psi_2^* \psi_1 + \psi_1^* \psi_2) dx, \quad (13)$$

$$P_y = \int_{-\infty}^{+\infty} i(\psi_2^* \psi_1 - \psi_1^* \psi_2) dx, \quad (14)$$

$$P_z = \int_{-\infty}^{+\infty} (\psi_1^* \psi_1 - \psi_2^* \psi_2) dx. \quad (15)$$

For the initial and final times  $P_z(0) = 1$  and  $P_z(t_f) = -1$ , corresponding to the spin-up and spin-down states, respectively, as shown in Fig. 4. The spatial orthogonality of the eigenstates leads to zero  $P_x$  and  $P_y$  during the operation time, indicating that the transfer occurs along mixed states in the spin subspace (see Fig. 5), although the auxiliary invariant-based trajectory describes the motion of a pure state on the surface of the Bloch sphere.

To check the applicability of this effective two-level system, we calculate a ‘‘multilevel’’ spinor wave function  $\psi^m(x, t)$  by direct numerical integration of the time-dependent Schrödinger equation with Hamiltonian (3) and  $\Delta(t), \Omega(t)$

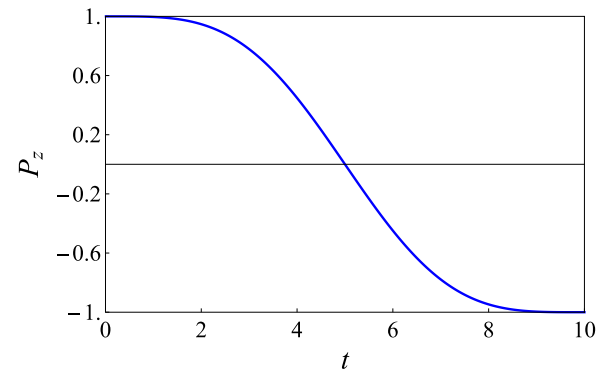


FIG. 4. (Color online) Time evolution of the  $z$  component of spin polarization  $P_z$ . Parameters are the same as in Fig. 3.

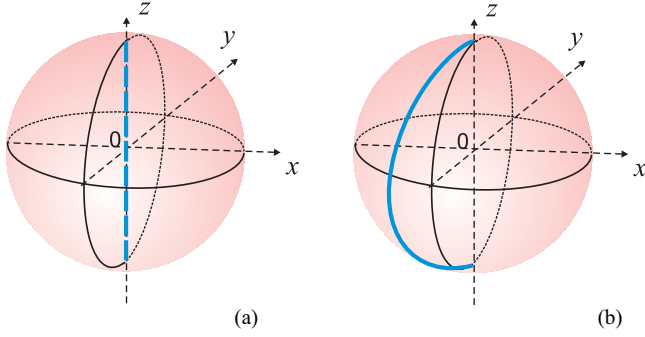


FIG. 5. (Color online) Trajectory of state evolution [thick (blue) line] inside the Bloch sphere in the spin subspace (a) and on the Bloch sphere in the total space (b).

given by Eqs. (10) and (9). For the initial  $\psi^m(x,0) = \langle x|0\rangle|\uparrow\rangle$  [see Eq. (2)], the achieved fidelity  $F = |\langle 1, \downarrow | \psi^m(x, t_f) \rangle|^2$  is 0.9966 for  $c = 0.1$ , corresponding to a small  $\Delta E = 0.15$ . With increasing the energy gap in the two-level system, the influence of other states becomes more pronounced, and the fidelity decreases. However, high-fidelity transitions are still possible even for relatively large gaps. For example,  $F = 0.979$  for  $c = 1.5$ , corresponding to  $\Delta E = 2.25$ . The final density distributions for these two gaps are presented in Fig. 6, illustrating that the two-level approximation can be applied even when  $\Delta E$  is of the order of the distance between the orbital states.

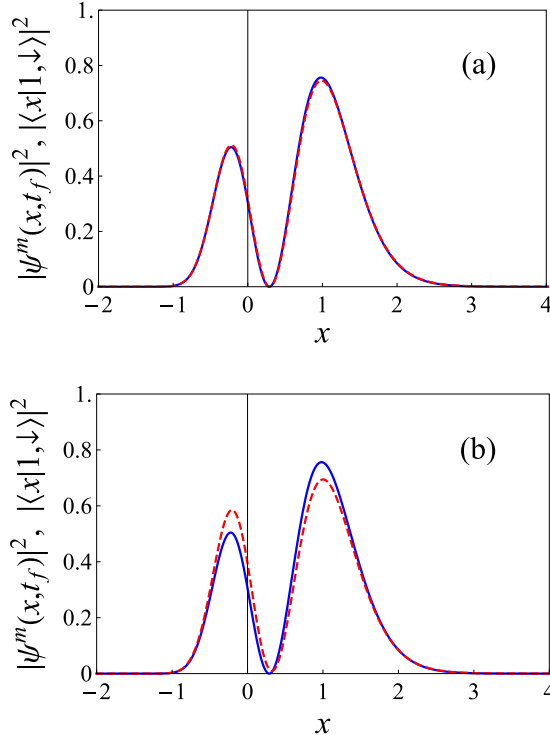


FIG. 6. (Color online) Norm square of  $|1, \uparrow\rangle$  [thick (blue) line] and  $\psi^m(x, t_f)$  [dashed (red) line] for  $c = 0.1$  (a) and  $c = 1.5$  (b).

#### IV. SCHEME 2: STATE TRANSITION BY TUNABLE SO-COUPLING DIRECTION AND TIME-DEPENDENT EFFECTIVE MAGNETIC FIELD

The state transition from  $|n, \uparrow\rangle$  to  $|l, \downarrow\rangle$  can be performed as well by a time-dependent Hamiltonian,

$$\mathcal{H} = \frac{p^2}{2} + U(x) + \alpha p(\boldsymbol{\sigma} \cdot \mathbf{n}_1) + \frac{\beta(t)}{2}(\boldsymbol{\sigma} \cdot \mathbf{n}_2), \quad (16)$$

where  $\boldsymbol{\sigma}$  is the Pauli matrix vector, and  $\beta(t)$  is an effective Zeeman splitting induced by an effective magnetic field in the  $\mathbf{n}_2$  direction. The SO coupling and the effective magnetic field are applied in the directions  $\mathbf{n}_1 = (\sin \theta_1 \cos \varphi_1, \sin \theta_1 \sin \varphi_1, \cos \theta_1)$  and  $\mathbf{n}_2 = (\sin \theta_2 \cos \varphi_2, \sin \theta_2 \sin \varphi_2, \cos \theta_2)$ , respectively. The polar and azimuthal angles  $\theta_j$  and  $\varphi_j$  ( $j = 1, 2$ ) are tunable parameters.

##### A. Noninteracting atoms

First, we consider noninteracting atoms and construct the  $2 \times 2$  Hamiltonian for the two-level system by taking the matrix elements of  $\mathcal{H}$  [Eq. (16)] in the basis of  $|n, \uparrow\rangle, |l, \downarrow\rangle$ ,

$$H(t) = \begin{bmatrix} E_n + \frac{\beta}{2} \cos \theta_2 & \mathcal{M} \\ \mathcal{M}^* & E_l - \frac{\beta}{2} \cos \theta_2 \end{bmatrix}, \quad (17)$$

where  $\mathcal{M} = (\alpha^2 G + \alpha K) \sin \theta_1 e^{-i\varphi_1} + \frac{\beta}{2} G \sin \theta_2 e^{-i\varphi_2}$ ,  $K = \langle n | e^{2i\alpha x} p | l \rangle$ , and the asterisk represents a complex conjugate. This scheme provides many possibilities for performing the state transfer. As an example, we set  $\theta_2 = \varphi_1 = \varphi_2 = 0$  and tune the angle  $\theta_1 \equiv \theta_1(t)$ , the direction of the SO-coupling field, and the effective Zeeman splitting  $\beta \equiv \beta(t)$ . We approximate  $\sin \theta_1 \approx \theta_1$ , and  $\cos \theta_1 \approx 1 - \theta_1^2/2$ . By symmetrizing the  $2 \times 2$  Hamiltonian in Eq. (17), we find the reduced form

$$\tilde{H}_0(t) = \frac{1}{2} \begin{bmatrix} Z & \tilde{X} + i\tilde{Y} \\ \tilde{X} - i\tilde{Y} & -Z \end{bmatrix}, \quad (18)$$

where  $\tilde{X} = 2\theta_1(t)\text{Re}[\mathcal{M}]$ ,  $\tilde{Y} = 2\theta_1(t)\text{Im}[\mathcal{M}]$ . Two equations for  $\theta_a$  and  $\varphi_a$  are obtained through the definition of the invariant, Eq. (5),

$$\theta_1(t) = -\frac{\dot{\theta}_a}{2|\mathcal{M}|\sin(\phi - \varphi_a)}, \quad (19)$$

$$\beta(t) = E_l - E_n - \dot{\varphi}_a - \frac{\dot{\theta}_a \cos \theta_a \cos(\phi - \varphi_a)}{\sin \theta_a \sin(\phi - \varphi_a)}, \quad (20)$$

where  $\tan \phi = \text{Im}[\mathcal{M}]/\text{Re}[\mathcal{M}]$ . The SO-coupling strength is fixed at  $\alpha = 1.6$ . By application of the same ansatz for  $\theta_a$  and  $\varphi_a$  as in Sec. III, we find the time dependence of two controllable variables  $\theta_1$  and  $\beta$  presented in Fig. 7. The geometry of directions and amplitudes corresponding to these two parameters is schematically illustrated in Fig. 7(c).

##### B. Interacting BEC

Now we consider transitions of the above type, taking into account interaction between the atoms, e.g., in the  $^{87}\text{Rb}$  condensate. The wave function  $\Psi(x, t) = (\Psi_\uparrow, \Psi_\downarrow)^T$ , normalized to the total number of condensate particles  $N$ ,

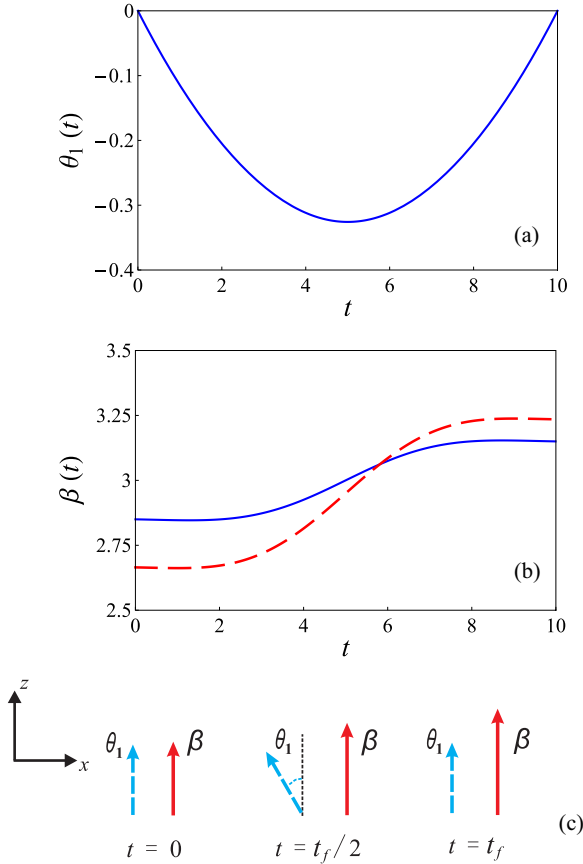


FIG. 7. (Color online) (a) Dependence of the angle  $\theta_1$  on the SO-coupling field for noninteracting or interacting atoms. (b) Effective Zeeman splitting  $\beta$  versus time  $t$ , without interaction [solid (blue) line] and with repulsive interaction  $g_{11} = 0.3$ ,  $g_{22} = 0.2$ ,  $g_{12} = g_{21} = 0.115$  [dashed (red) line]. (c) Schematic of the two controllable parameters  $\beta$  and  $\theta_1$  at  $t = 0$ ,  $t = t_f/2$ , and  $t = t_f$ . In all plots, the initial state is  $|0, \uparrow\rangle$  and the final one is  $|1, \downarrow\rangle$ . Other parameters are  $t_f = 10$ ,  $\alpha = 1.6$ , and  $c = 0.1$ .

satisfies the coupled Gross-Pitaevskii equations (GPEs):

$$\begin{aligned}
 i \frac{d\Psi_{\uparrow}}{dt} &= \left[ \frac{p^2}{2} + U(x) + \alpha p \cos \theta_1 + \frac{\beta(t)}{2} \cos \theta_2 + g_{\uparrow\uparrow} |\Psi_{\uparrow}|^2 \right. \\
 &\quad \left. + g_{\uparrow\downarrow} |\Psi_{\downarrow}|^2 \right] \Psi_{\uparrow} + \left( \alpha p \sin \theta_1 e^{-i\varphi_1} + \frac{\beta}{2} \sin \theta_2 e^{-i\varphi_2} \right) \Psi_{\downarrow}, \\
 i \frac{d\Psi_{\downarrow}}{dt} &= \left[ \frac{p^2}{2} + U(x) - \alpha p \cos \theta_1 - \frac{\beta(t)}{2} \cos \theta_2 + g_{\downarrow\downarrow} |\Psi_{\downarrow}|^2 \right. \\
 &\quad \left. + g_{\downarrow\uparrow} |\Psi_{\uparrow}|^2 \right] \Psi_{\downarrow} + \left( \alpha p \sin \theta_1 e^{i\varphi_1} + \frac{\beta}{2} \sin \theta_2 e^{i\varphi_2} \right) \Psi_{\uparrow}.
 \end{aligned} \quad (21)$$

The intra- and the intercomponent atomic interaction constants here are  $g_{jj}$  and  $g_{jk}$  ( $j \neq k = \uparrow, \downarrow$ ), respectively. As for the noninteracting gas, we also take  $\theta_1$  and  $\beta$  as controllable variables. (The scheme in Sec. II can be generalized similarly.) The inverse engineering based on a Lewis-Riesenfeld invariant is, however, not applicable, as Eq. (5) is not the invariant of

the new Hamiltonian  $H_1$  [ $\tilde{H}_0$  is given by Eq. (18)],

$$H_1 = \tilde{H}_0 + \begin{bmatrix} g_{11} |\psi_1|^2 + g_{12} |\psi_2|^2 & 0 \\ 0 & g_{21} |\psi_1|^2 + g_{22} |\psi_2|^2 \end{bmatrix}, \quad (22)$$

where the effective interaction factors are

$$\begin{aligned}
 g_{11} &= N g_{\uparrow\uparrow} Q(0,0), & g_{22} &= N g_{\downarrow\downarrow} Q(1,1), \\
 g_{12} &= N g_{\uparrow\downarrow} Q(0,1), & g_{21} &= N g_{\downarrow\uparrow} Q(0,1),
 \end{aligned}$$

where

$$Q(n,l) = \int_{-\infty}^{\infty} |\langle x|n\rangle|^2 |\langle x|l\rangle|^2 dx \quad (23)$$

and  $n, l$  are the orbital quantum numbers. For the given choice of the initial and final states, we obtain, with the wave functions in Eq. (2), the ratios  $Q(0,0)/Q(1,1) = 1.5$  and  $Q(0,1)/[Q(0,0) + Q(1,1)] = 0.23$ . By setting the same value for  $g_{\uparrow\uparrow}$ ,  $g_{\uparrow\downarrow}$ ,  $g_{\downarrow\uparrow}$ , and  $g_{\downarrow\downarrow}$ , we finally determine  $g_{11}$ ,  $g_{22}$ ,  $g_{12}$ , and  $g_{21}$ .

For this nonlinear system, inverse engineering is still feasible by means of the ansatz

$$\psi(t) = \begin{pmatrix} \cos \frac{\theta_p}{2} e^{i\varphi_p/2} \\ \sin \frac{\theta_p}{2} e^{-i\varphi_p/2} \end{pmatrix} e^{i\gamma}, \quad (24)$$

where  $\gamma$ , an auxiliary parameter, is the global phase.

Choosing for  $\theta_p$  and  $\varphi_p$  the same ansatz as above for  $\theta_a$  and  $\varphi_a$ , we obtain from the GPE

$$\begin{aligned}
 \theta_1(t) &= -\frac{\dot{\theta}_p}{2|\mathcal{M}| \sin(\phi - \varphi_p)}, \quad (25) \\
 \beta(t) &= E_l - E_n - \dot{\varphi}_p - \frac{\dot{\theta}_p \cos \theta_p \cos(\phi - \varphi_p)}{\sin \theta_p \sin(\phi - \varphi_p)} \\
 &\quad - g_{11} \cos^2 \frac{\theta_p}{2} - g_{12} \sin^2 \frac{\theta_p}{2} \\
 &\quad + g_{22} \sin^2 \frac{\theta_p}{2} + g_{21} \cos^2 \frac{\theta_p}{2}. \quad (26)
 \end{aligned}$$

The function  $\theta_1$  in Eq. (25) keeps the same form as that without the interaction [Eq. (19)], as shown in Fig. 7(a). In contrast, including the interaction in the diagonal terms results in changes in the amplitude of the external effective magnetic field, as shown in Fig. 7(b). In other words, the modulation in  $\beta$  compensates for the contribution of nonlinear terms.

## V. ROBUSTNESS

We now test the stability of the protocol based on Hamiltonian (22) with respect to variations in the effective magnetic field caused by systematic errors and noise, which induce shifts in the diagonal terms. First, we consider the effective Zeeman splitting, which deviates from the nominal value in Hamiltonian (22) as  $\beta^{\text{real}} = \beta(1 + \lambda)$ , where  $\lambda$  is a constant.

The fidelity  $F = |\langle l, \downarrow | \psi(t_f) \rangle|^2$  with respect to  $\lambda$  is compared for noninteracting and interacting condensates in Fig. 8, demonstrating the stability around  $\lambda = 0$ .

Besides the systematic errors, we consider a noisy perturbation, i.e., Hamiltonian  $H_1$  [Eq. (22)] perturbed by a stochastic

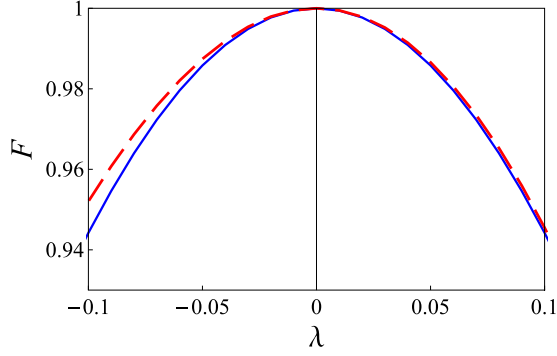


FIG. 8. (Color online) Fidelity with respect to the relative error in the magnetic field  $\lambda$  for noninteracting condensates [solid (blue) line] and for repulsive interaction,  $g_{11} = 0.3$ ,  $g_{22} = 0.2$ ,  $g_{12} = g_{21} = 0.115$  [dashed (red) line].

term,  $H^n$ . The GPE is modified as

$$i \frac{d\Psi(t)}{dt} = (H_1 + H^n)\Psi(t), \quad (27)$$

where  $H^n = \lambda' H' \xi(t)$ ,  $\langle \xi(t) \rangle = 0$ ,  $\langle \xi(t) \xi(t') \rangle = \delta(t - t')$ ,  $\lambda'$  is the noise strength, and  $H'$  is

$$H' = \frac{1}{2} \begin{bmatrix} \beta & 0 \\ 0 & \beta \end{bmatrix}. \quad (28)$$

The density matrix now obeys Eq. (24):

$$\dot{\rho} = -i[H_1, \rho] - \frac{\lambda'^2}{2} [H', [H', \rho]]. \quad (29)$$

We introduce the Bloch vector with components  $u = \rho_{1-1} + \rho_{-11}$ ,  $v = -i(\rho_{1-1} - \rho_{-11})$ , and  $w = \rho_{11} - \rho_{-1-1}$  and obtain

$$\begin{aligned} \dot{u} &= -\frac{1}{2}\lambda'^2 \Delta^2 u + (Z + g_d + g_s w - g'_s w + g'_d)v - Yw, \\ \dot{v} &= (-Z - g_d - g_s w - g'_d + g'_s w)u - \frac{1}{2}\lambda'^2 \Delta^2 v + Xw, \\ \dot{w} &= Yu - Xv, \end{aligned} \quad (30)$$

where  $g_d = (g_{11} - g_{22})/2$ ,  $g_s = (g_{11} + g_{22})/2$ ,  $g'_d = (g_{12} - g_{21})/2$ ,  $g'_s = (g_{12} + g_{21})/2$ . We calculate the fidelity numerically in Fig. 9, which, again, shows stability around  $\lambda = 0$ .

For both types of perturbations the stability region where the fidelity is close enough to 1 may be broadened as proposed in Ref. [24].

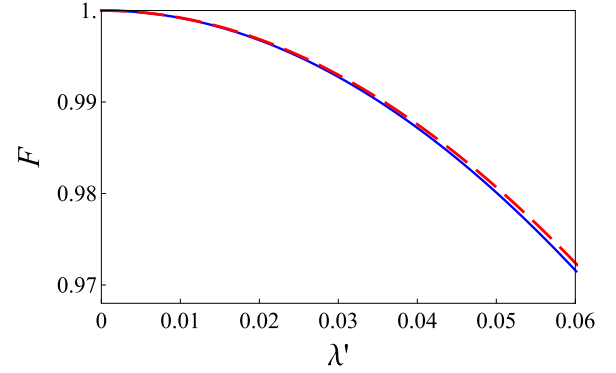


FIG. 9. (Color online) Fidelity with respect to  $\lambda'$  for noninteracting [solid (blue) line] and repulsive interaction  $g_{11} = 0.3$ ,  $g_{22} = 0.2$ ,  $g_{12} = g_{21} = 0.115$  [dashed (red) line].

## VI. SUMMARY

We have proposed several invariant-based inverse engineering schemes for the state transfer of SO-coupled bosons trapped in a Morse potential. For noninteracting atoms, the time dependence of Raman coupling and detuning are designed to transfer orbital and spin states simultaneously. Due to the asymmetry of the Morse potential, this transfer leads to a spatial displacement of the atomic wave, which, as a result, allows for the simultaneous control of the condensate coordinate and spin. An alternative scheme for the state transfer is to tune the direction of the SO-coupling field and the Zeeman coupling strength. For an interacting BEC, the amplitude of the effective magnetic field can be designed to compensate for the interaction-related nonlinearity in the GPEs. The proposed protocols are stable with respect to systematic errors and amplitude noise in the applied effective magnetic field. Similar ideas may be applied to design fast transitions between a bound state and the continuum.

## ACKNOWLEDGMENTS

This work was partially supported by the NSFC (Grants No. 11474193, No. 61404079, and No. 61176118), the Shanghai Municipal Science and Technology Commission (Grants No. 13PJ1403000 and No. 14YF1408400), the Specialized Research Fund for the Doctoral Program (Grant No. 2013310811003), the Program for Eastern Scholars, the Basque Country Government (Grants No. IT472-10), Ministerio de Economía y Competitividad (Grant No. FIS2012-36673-C03-01), and UPV/EHU program UFI 11/55.

- [1] R. Bücker, T. Berrada, S. van Frank, J.-F. Schaff, T. Schumm, J. Schmiedmayer, G. Jäger, J. Grond, and U. Hohenester, *J. Phys. B: At. Mol. Opt. Phys.* **46**, 104012 (2013).  
 [2] S. Martínez-Garaot, E. Torrontegui, X. Chen, M. Modugno, D. Guéry-Odelin, S. Y. Tseng, and J. G. Muga, *Phys. Rev. Lett.* **111**, 213001 (2013).  
 [3] Y. Ban and E. Y. Sherman, *Phys. Rev. A* **85**, 052130 (2012).

- [4] D. Sokolovski and E. Ya. Sherman, *Phys. Rev. A* **89**, 043614 (2014).  
 [5] T. D. Stanescu, B. Anderson, and V. Galitski, *Phys. Rev. A* **78**, 023616 (2008).  
 [6] Y. J. Lin, K. Jiménez-García, and I. B. Spielman, *Nature* **471**, 83 (2011).  
 [7] X.-J. Liu, M. F. Borunda, X. Liu, and J. Sinova, *Phys. Rev. Lett.* **102**, 046402 (2009).

- [8] P. Wang, Z.-Q. Yu, Z. Fu, J. Miao, L. Huang, S. Chai, H. Zhai, and J. Zhang, *Phys. Rev. Lett.* **109**, 095301 (2012).
- [9] L. W. Cheuk, A. T. Sommer, Z. Hadzibabic, T. Yefsah, W. S. Bakr, and M. W. Zwierlein, *Phys. Rev. Lett.* **109**, 095302 (2012).
- [10] J. Dalibard, F. Gerbier, G. Juzeliunas, and P. Ohberg, *Rev. Mod. Phys.* **83**, 1523 (2011).
- [11] H. Zhai, *Int. J. Mod. Phys.* **26**, 1230001 (2012).
- [12] V. Galitski and I. B. Spielman, *Nature* **494**, 49 (2013).
- [13] T. Yu and M. W. Wu, *Phys. Rev. A* **88**, 043634 (2013).
- [14] C. L. Qu, C. Hamner, M. Gong, C. W. Zhang, and P. Engels, *Phys. Rev. A* **88**, 021604 (2013).
- [15] Y. C. Zhang, S. W. Song, C. F. Liu, and W. M. Liu, *Phys. Rev. A* **87**, 023612 (2013).
- [16] A. J. Olson, S. J. Wang, R. J. Niffenegger, C. H. Li, C. H. Greene, and Y. P. Chen, *Phys. Rev. A* **90**, 013616 (2014).
- [17] X. Chen, A. Ruschhaupt, S. Schmidt, A. del Campo, D. Guéry-Odelin, and J. G. Muga, *Phys. Rev. Lett.* **104**, 063002 (2010).
- [18] E. Torrontegui, S. Ibáñez, S. Martínez-Garaot, M. Modugno, A. del Campo, D. Guéry-Odelin, A. Ruschhaupt, X. Chen, and J. G. Muga, *Adv. At. Mol. Opt. Phys.* **62**, 117 (2013).
- [19] Y. Ban, X. Chen, E. Ya. Sherman, and J. G. Muga, *Phys. Rev. Lett.* **109**, 206602 (2012).
- [20] P. M. Morse, *Phys. Rev.* **34**, 57 (1929).
- [21] For realistic parameters  $a = 0.1/\mu\text{m}$ ,  $A = 10\hbar^2 a^2/M$ , and  $M$  for the  $^{87}\text{Rb}$  atom one obtains estimates  $\omega \sim 20 \text{ s}^{-1}$  and  $l_c \sim 5 \mu\text{m}$ .
- [22] Y. Colombe, D. Kadio, M. Olshani, B. Mercier, V. Lorent, and H. Perrin, *J. Opt. B* **5**, S155 (2003).
- [23] H. R. Lewis and W. B. Riesenfeld, *J. Math. Phys.* **10**, 1458 (1969).
- [24] A. Ruschhaupt, X. Chen, D. Alonso, and J. G. Muga, *New J. Phys.* **14**, 093040 (2012).